

2

Ca and K Isotope Fractionation by Diffusion in Molten Silicates: Large Concentration Gradients Are Not Required to Induce Large Diffusive Isotope Effects

James M. Watkins¹, John N. Christensen², Donald J. DePaolo^{2,3}, and Frederick J. Ryerson⁴

ABSTRACT

Laboratory experiments were used to investigate diffusive isotopic fractionation of calcium and potassium in phonolite-rhyolite diffusion couples. The starting compositions have very different SiO₂ and K₂O, but similar CaO. These were juxtaposed and held in a completely molten state at 1450°C and 1.0 GPa for durations of 2.5 or 6 hours in a piston cylinder apparatus. The resulting major-element diffusion profiles exhibit many complexities, including uphill diffusion of all major oxide components. The diffusive fluxes for SiO₂, K₂O, and CaO were modeled using a published modified effective binary diffusion model, whereby diffusion is driven by activity gradients that are solely a function of the time-evolving SiO₂ concentration. Both Ca and K exhibit large diffusive isotope effects that can be explained by imposing a mass dependence on the diffusion coefficients used to model the major-element profiles. The mass dependence is parameterized in terms of the inverse ratio of the isotope masses raised to an empirically determined exponent β (i.e., $D_i/D_j = [m_j/m_i]^\beta$). Our results confirm that β factors vary depending on the element as well as liquid composition, and that large diffusive isotope effects can arise even in the absence of a large initial concentration gradient. The retrieved β factor for Ca (0.10 ± 0.02) is typical of Ca in natural silicate liquids, whereas the β factor for K (0.25 ± 0.03) is the highest value yet reported, suggesting that large diffusive K isotope effects may yet be found in high- T environments.

2.1. INTRODUCTION

Igneous and metamorphic rocks exhibit stable isotope variations in excess of what can reasonably be attributed to mixing processes or equilibrium partitioning during partial

melting and (re)crystallization. Experimental studies have shown that diffusion is capable of generating measurable (sub-permil) to large (tens of permil) kinetic isotopic fractionations that can account for some of this variability, and detailed knowledge of these effects can yield unique insights into the molecular level controls on diffusive transport and the role of kinetics in the formation of minerals in high temperature settings (Antonelli et al., 2019b; Barrat et al., 2005; Beck et al., 2006; Chen et al., 2018; Chopra et al., 2012; Dauphas, 2007; Dauphas et al., 2010; Gallagher & Elliott, 2009; Gao et al., 2011; Jeffcoate et al., 2007; Kil et al., 2016; Lundstrom et al., 2005; Marschall et al., 2007; Mueller et al., 2014; Oeser et al., 2015; Parkinson et al., 2007; Richter et al., 2009, 2014, 2016, 2017; Roskosz et al., 2006; Rudnick & Ionov, 2007; Sio et al., 2013;

¹Department of Earth Sciences, University of Oregon, Eugene, Oregon, USA

²Earth and Environmental Science Area, Energy Geosciences Division, Lawrence Berkeley National Laboratory, Berkeley, California, USA

³Department of Earth and Planetary Science, University of California, Berkeley, California, USA

⁴Atmospheric, Earth, and Energy Division, Lawrence Livermore National Laboratory, Livermore, California, USA

Su et al., 2016; Teng et al., 2006, 2011; Wu et al., 2018; Zhao et al., 2017).

Current knowledge of diffusive isotopic fractionations in molten silicates is based on a few elements (Ca, Fe, Mg, Li, and Si) and silicate melt compositions (cf. Watkins et al., 2017, for a review). The mass dependence on diffusion coefficients varies between cations and with liquid composition. In basalt-rhyolite diffusion couples, for example, the stable isotopes of major elements (Ca, Fe, Mg) exhibit less mass discrimination ($\beta < 0.075$) than the stable isotopes of trace element Li ($\beta \approx 0.215$) (Richter et al., 2003, 2009; Watkins et al., 2009). In simplified silicate liquids, it has been found that the β factor for Ca and Mg varies between 0.05 and 0.21, depending on liquid composition, and is correlated with the “solvent-normalized” diffusivity (e.g., $D_{\text{Ca}}/D_{\text{Si}}$), suggesting that faster diffusing elements exhibit greater mass discrimination because they move as single atoms or small moieties whose diffusion is decoupled from that of the major melt structures/components (Goel et al., 2012; Watkins et al., 2009, 2011). This simple relationship provides a useful framework for choosing an appropriate value for β in diffusion models and for predicting where there might be large diffusive isotope effects in nature.

In this contribution, we present results from new diffusion couple experiments with two motivating factors in mind. First, the solvent-normalized diffusivity can only be defined in situations where there is a large initial concentration gradient for the component of interest and an effective binary diffusion model is applicable. And yet, we are aware that large diffusive isotope effects can arise even in the absence of large initial concentration gradients. One such example is in ugandite-rhyolite diffusion couple experiments where Ca isotopes were fractionated by $\sim 2\%$ due to diffusive coupling of CaO with Al_2O_3 (Watkins et al., 2009). Such strong multicomponent diffusion effects warrant further investigation because they may contribute to isotope variations within and among minerals formed in high- T settings. Second, the ratio D_i/D_{Si} tends to be lower and approach unity for elements that are present in major quantities because the net flux of a major element requires cooperative motion of the other major components of the liquid. The β factor for Li can be high because it diffuses fast, and it can diffuse fast because it is present in trace quantities. The same may be true for Ca; the β factor for Ca approaches that of Li in experiments where Ca is present in minor quantities (~ 2 wt%; Watkins et al., 2011). These observations raise the question of whether the (typically) fast-diffusing K_2O component will behave like Li and have a high β factor or whether it will behave like other major elements and have a β factor closer to zero.

2.2. METHODS

2.2.1. Experiments

Two rock compositions used for the diffusion couple experiments were chosen on the basis of being as different from each other as possible while having similar CaO but different K_2O . The compositions that best matched these criteria are a high-CaO rhyolite with 70 wt% SiO_2 and a phonolite with 55 wt% SiO_2 (Table 2.1). The rhyolite was supplied by Shaun Brown and comes from Chuginadak Island in the Aleutians (Sample ID FMI-6; Yododzinski et al., 2010) and the phonolite was collected in 2002 by JMW from the northern Black Hills tertiary magmatic province. The two compositions have nearly identical CaO (2.9 wt% versus 3.0 wt%) and the large difference in SiO_2 is balanced mostly by the extremely high K_2O (10.4 wt%) and high Al_2O_3 (19 wt%) of the phonolite (Figure 2.1).

Approximately 0.055 grams of rock powder from each sample were tamped into a graphite capsule, with the higher density phonolite on the bottom to ensure gravitational stability. The capsule was capped with a graphite plug and graphite lid and loaded into a standard 3/4-inch piston-cylinder assembly (Fig. 2.2). The assembly was cold-pressurized to 12.8 kbar and then brought to 1450°C at a ramp rate of 150°C/min. During the ramp, pressure increased initially due to thermal expansion but ultimately decreased to nearly the target pressure of 10 kbar and was brought to the target pressure through manual adjustments. Once the target temperature was reached, it was held at constant temperature ($\pm 2^\circ\text{C}$) and pressure (± 0.2 kbar) for the dwell time. To end a run, the power was turned off and the sample cooled to below the glass transition within a few seconds and to 130°C in about 30 seconds.

Table 2.1 Major element composition of starting materials (fused glasses) measured by electron microprobe.

Oxide	Rhyolite (n=13 spots)	Phonolite (n=14 spots)
SiO_2	70.06	54.88
Al_2O_3	14.75	19.10
CaO	2.88	3.01
FeO	3.93	4.93
MgO	0.89	1.38
K_2O	2.86	10.43
Na_2O	5.39	5.47
TiO_2	0.59	0.90
P_2O_5	0.10	0.35
MnO	0.08	0.10
Total	101.09	100.27

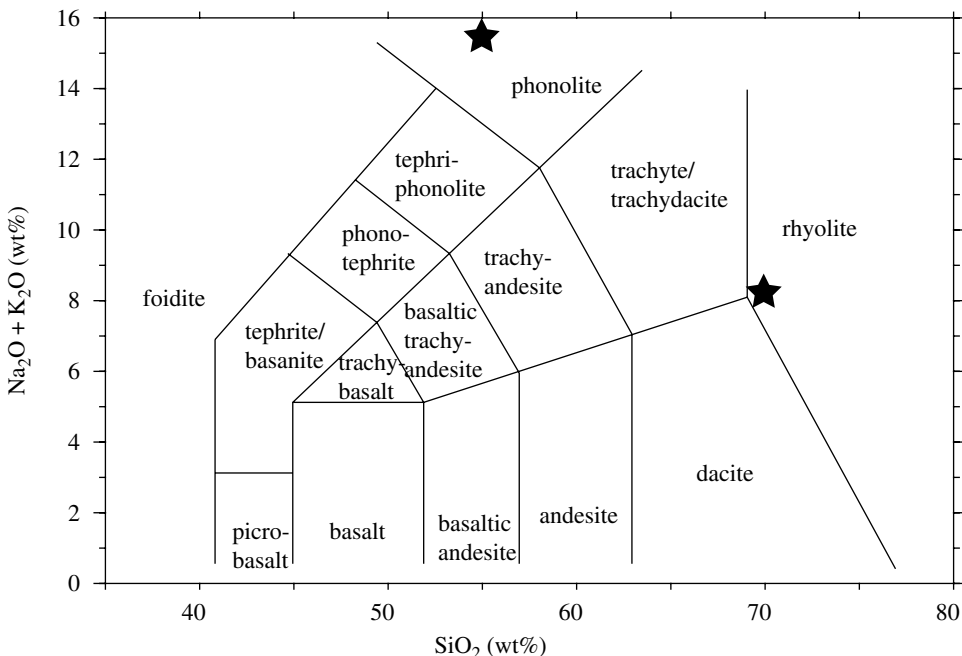


Figure 2.1 Alkali-silica diagram showing the coordinates of the two starting materials used in the diffusion couple experiments.

2.2.2. Electron Microprobe Analyses

Each diffusion couple was extracted and sectioned down its vertical axis, mounted in a 1-inch epoxy puck, and polished to $0.25\text{ }\mu\text{m}$. After mounting, we measured the length of the diffusion couples and note that each one had compressed from an initial length of 10.4 mm down to about 6.6 mm. Axis-parallel major-element diffusion profiles were measured from end-to-end with a JEOL JXA-8200 SuperProbe at Lawrence Livermore National Laboratory using a 15 nA beam current rastered at $12000\times$ magnification ($12\text{ }\mu\text{m} \times 9\text{ }\mu\text{m}$ beam dimensions) with an accelerating voltage of 15 kV. Sodium was measured first at each spot to mitigate effects of Na migration. All electron probe data are provided as an Excel file in the Electronic Supplement.

2.2.3. Ca Isotopic Measurements

After microprobe measurements, diffusion couples were sectioned into wafers, about $465\text{ }\mu\text{m}$ thick and weighing about 3 mg, using a Bico diamond wafer saw with blade thickness of $165\text{ }\mu\text{m}$. The wafers were dissolved in a mixture of hydrofluoric and perchloric acid, dried at 165°C , redissolved in 5 mL 3N HNO_3 , aliquotted, mixed with a ^{42}Ca - ^{48}Ca double spike to correct for spectrometer-induced mass discrimination

(cf. Watkins, 2010), dried to a small bead, and the bead was redissolved in $100\text{ }\mu\text{L}$ 3N HNO_3 for loading onto cation exchange columns. The Ca fraction was separated and collected by cation exchange chromatography using Eichrom Ca-spec DGA resin. The non-Ca fraction was saved for subsequent K isotope work. About $3\text{ }\mu\text{g}$ of purified Ca from each sample were loaded onto a zone-refined Re filament, dried down, topped with $1\text{ }\mu\text{L}$ of 20% of H_3PO_4 acid and re-dried.

Ca isotopes were measured by thermal ionization mass spectrometry (TIMS) at UC-Berkeley on a Thermo-Finnigan Triton TI with nine moveable Faraday collectors. For each sample, at least 100 isotope ratio measurements were made to reduce within-run uncertainties to $\pm 0.04\text{\textperthousand}$. At the time these data were collected in 2009, the long-term uncertainty in the standard (SRM 715) was conservatively estimated to be $\pm 0.15\text{\textperthousand}$, and we use this value for the error bars. The Ca isotope ratios of the samples were determined using an iterative spike subtraction algorithm and are reported as (Skulan et al., 1997):

$$\delta^{44}\text{Ca, \textperthousand} = \left(\frac{^{44}\text{Ca} / ^{40}\text{Ca}}{0.0212076} - 1 \right) \cdot 1000. \quad (2.1)$$

The Ca isotope compositions are provided in Table 2.2.

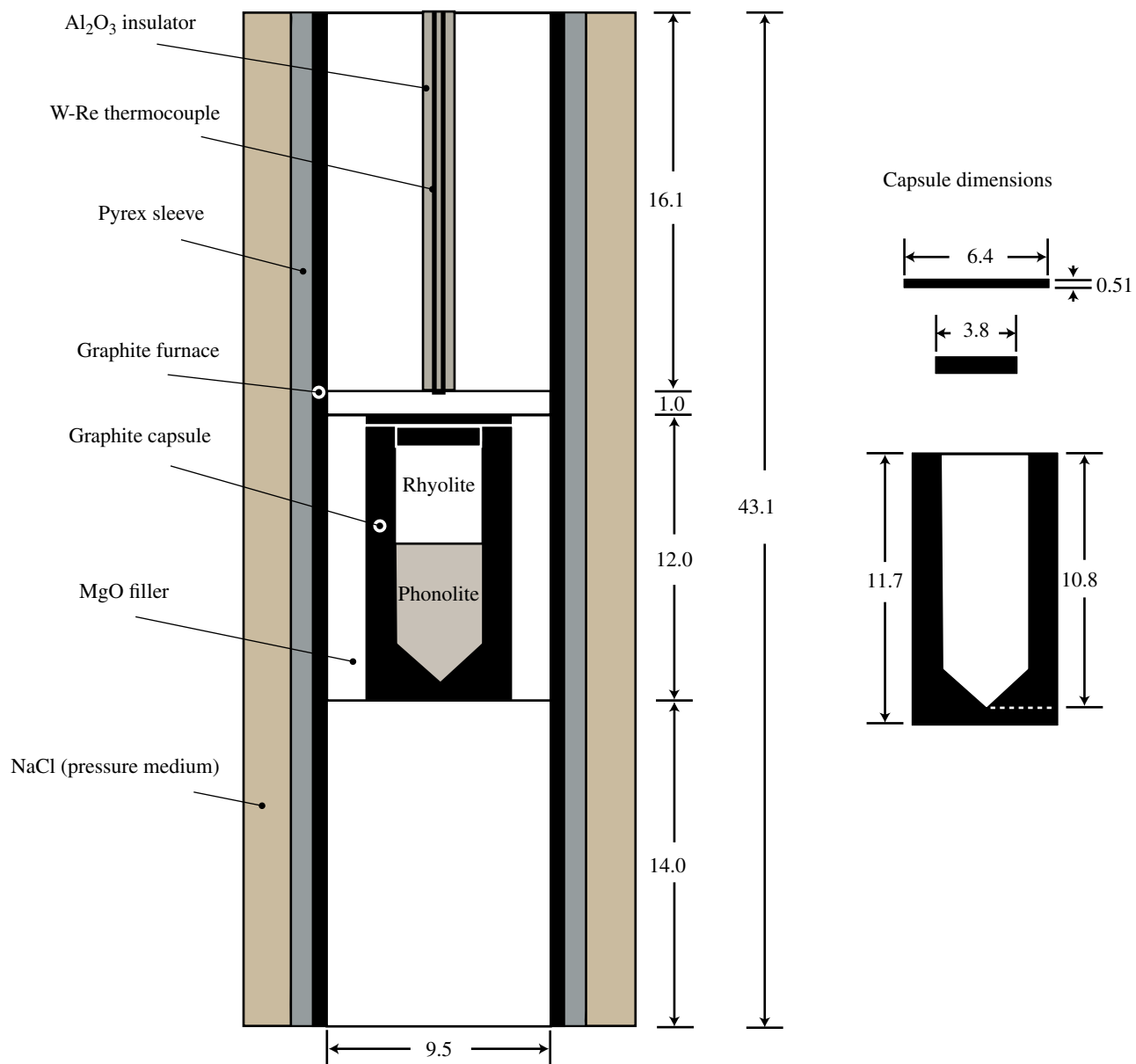


Figure 2.2 Piston-cylinder sample assembly used for the diffusion couple experiments. All dimensions are in millimeters.

2.2.4. K Isotopic Measurements

Potassium was separated for isotopic analysis from the sample solutions after Ca separation using columns loaded with 1.8 ml of AG30x8 cation resin. Sample aliquots with ~600 ng K were dried down, taken up in 300 μ L of 1 M HNO₃, loaded on the columns, eluted with 1 M HNO₃, and the K fraction was collected (Bourg et al., 2010). After drying the separated K solutions down, the K residue was brought up in 0.3 N HNO₃ to a concentration of 400 ppb. The ⁴¹K/³⁹K ratios of the separated K were measured using a multi-collector ICP

sourced mass spectrometer (IsoProbe, GV Instruments Ltd.) at Lawrence Berkeley National Lab. The IsoProbe is equipped with a RF hexapole ion-guide that allows the introduction of gasses to provide both energy focusing as well the removal of isobaric interferences arising from Ar ions. In the case of the K isotopic measurements reported here, He and H₂ were introduced to the hexapole region at rates of 10 mL/min and 1 mL/min, respectively, to suppress mass interferences from Ar isotopes. For K isotopic measurements, a standard-sample bracketing technique was employed using an in-house K reference (K spectroscopic standard, ULTRA Scientific) matching the sample

Table 2.2 Summary of isotopic results.

Sample	Distance (mm)	$\delta^{44}\text{Ca}$	n	$\delta^{41}\text{K}$	n
RP2-1	0.33	0.70	2	–	–
RP2-2	0.99	0.46	5	–	–
RP2-3	1.65	0.15	4	–	–
RP2-4	2.31	-0.37	2	–	–
RP2-5	2.97	-0.77	2	–	–
RP2-6	3.62	-0.90	2	–	–
RP2-7	4.28	-1.26	2	–	–
RP2-8	4.94	-0.78	2	–	–
RP2-9	5.60	-0.78	2	–	–
RP2-10	6.26	–	–	–	–
RP3-1	0.33	-0.42	3	-2.35	–
RP3-2	0.98	-0.62	3	-3.47	–
RP3-3	1.63	0.01	2	-4.19	–
RP3-4	2.28	0.95	2	-2.44	–
RP3-5	2.93	0.68	2	-1.2	–
RP3-6	3.59	-0.68	2	0.54	–
RP3-7	4.24	-0.78	2	1.01	–
RP3-8	4.89	-0.91	2	1.38	–
RP3-9	5.54	-0.76	2	1.59	–
RP3-10	6.19	–	–	–	–
Rhyolite	–	-0.29	3	–	–
Phonolite	–	-0.36	4	–	–

unknowns in concentration (Christensen et al., 2018). The potassium isotopic composition is reported as:

$$\delta^{41}\text{K}, \text{\%} = \left(\frac{(^{41}\text{K} / ^{39}\text{K})_{\text{sample}}}{(^{41}\text{K} / ^{39}\text{K})_{\text{reference}}} - 1 \right) \cdot 1000, \quad (2.2)$$

where $(^{41}\text{K} / ^{39}\text{K})_{\text{reference}}$ is the average of the two bracketing analyses of the K reference solution prior to and after the analysis of the sample. The sample solutions were introduced to the IsoProbe using an Aridus II (Cetac Technologies) desolvation system with a Teflon nebulizer with a measured uptake of 60 microlitres/minute. Approximately 150 ng of K was used per isotopic analysis run. The typical uncertainty in $\delta^{41}\text{K}$ is conservatively given as $\pm 0.3\%$ and is based on the combined uncertainties in the measured $^{41}\text{K} / ^{39}\text{K}$ of the bracketing reference and samples. Further details on the mass spectrometry technique can be found in Richter et al. (2011).

2.3. RESULTS

2.3.1. Major Element Diffusion Profiles

Major-element diffusion profiles from two experiments that differ in duration (2.5 versus 6 hours) are shown in Fig. 2.3. Note that the x-coordinates of both profiles have been shifted such that the phonolite-rhyolite interfaces overlap and the profiles are framed within each panel.

Additionally, in the 6-hour experiment the capsule was loaded with more phonolite powder (0.07 g) than rhyolite powder (0.04 g), and consequently, the rhyolite side of the couple is short, occupying only about one-third of the capsule length.

The major element profiles exhibit features that are interesting, although we cannot fully explain some of them. We observe uphill diffusion (i.e., diffusion of a component against its own concentration gradient) in all the major-element oxides, including SiO_2 . The SiO_2 and Al_2O_3 profiles change relatively little from the starting materials, which is expected because of the low diffusivities of these components and the coupling between Si and Al in the silicate framework components of the liquids. One thing that is unexpected is that the absolute concentrations of SiO_2 and Al_2O_3 on the rhyolite end of the profiles are low relative to the starting values. This should be regarded as an analytical inconsistency as it cannot be explained by a dilution effect. The absolute concentrations of Na_2O are even more problematic, being too high relative to the starting materials. The simplest explanation is that the starting materials actually had Na_2O concentrations that were about 0.5% higher than reported. This is unexpected, but possible, since it is well known that Na can be volatilized during EMP analysis, leading to incorrectly low measured concentrations. These issues do not significantly affect the main conclusions that we draw from the Ca and K isotopic results.

A notable feature of the data is the dramatic rearrangement of the Na, Ca, and K components in the 2.5 hour run. The K profile is strongly affected by rapid diffusion of K from the phonolite to the rhyolite, producing a steep K concentration profile in the rhyolite. The large increase in K in the rhyolite, especially close to the contact with phonolite, is accommodated mostly by rapid diffusion of Ca and some Na from the rhyolite to the phonolite. Apparently, as the Ca gradient becomes steep within the rhyolite, Na diffuses both into the phonolite, and toward the rhyolite end of the capsule to maintain a near-constant Na/Ca within the rhyolite. We have not attempted to capture this coupling in our modeling of Ca (see Section 2.5), but since Na diffuses rapidly, its movement probably does not greatly affect the diffusion of Ca. The Na/Ca ratio (or Ca/(Ca+Na) ratio) is nearly constant within the rhyolite, and within the phonolite, which is a clear indication that both Na and Ca diffuse quickly to what must be thermodynamically favored Na/Ca ratios that are presumably determined largely by the SiO_2 ($\pm \text{Al}_2\text{O}_3$) of the two liquids.

2.3.2. Ca and K Isotopes

The phonolite-rhyolite diffusion couples produced large diffusive isotope effects in both Ca (Fig. 2.4a) and K (Fig. 2.4b). For Ca isotopes, the felsic side is enriched

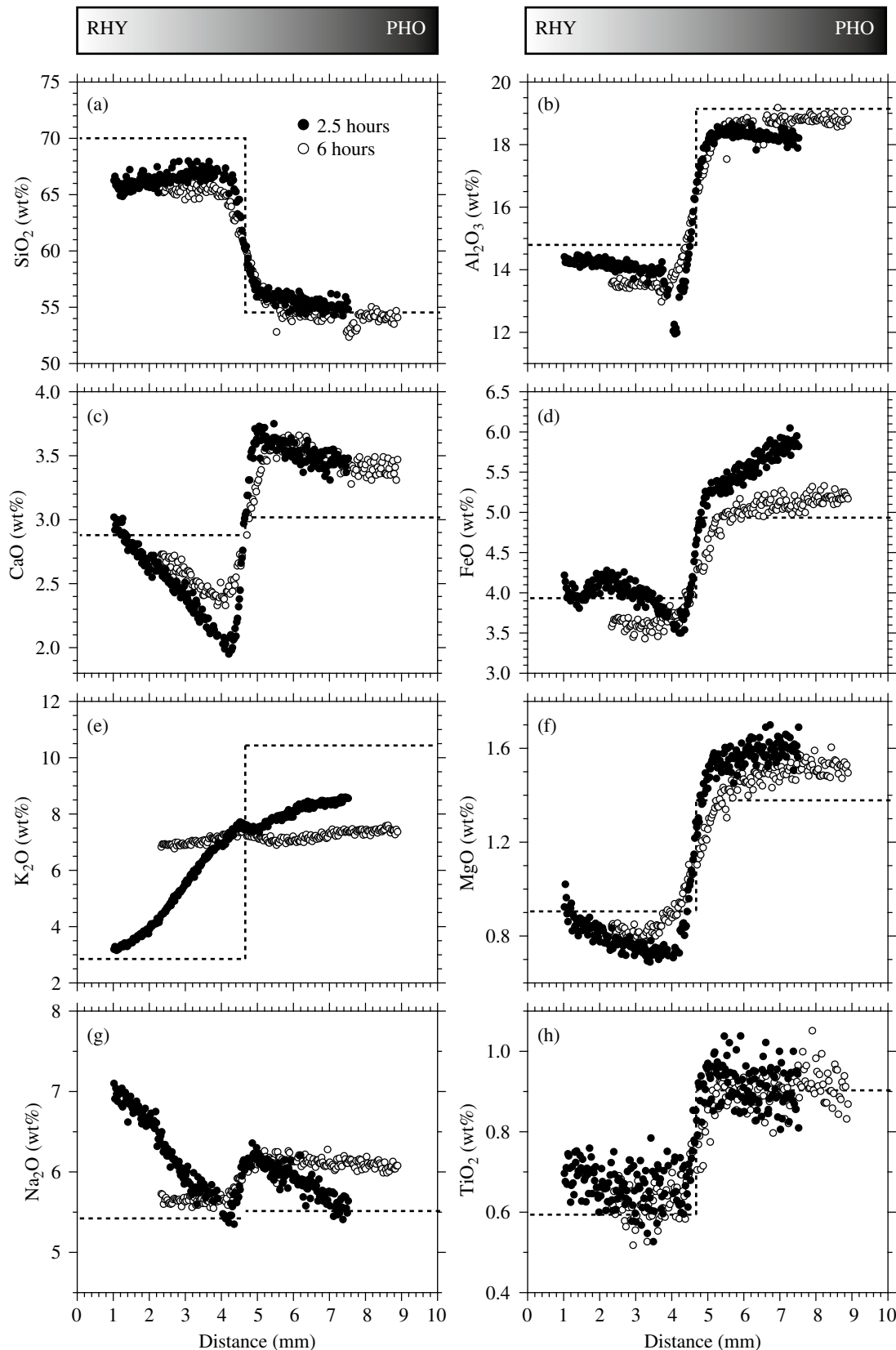


Figure 2.3 Major-element diffusion profiles from two experiments lasting 2.5 hours and 6 hours. Note that the data have been shifted to the right by 1 mm and 2.3 mm for the 2.5 hour and 6 hour runs, respectively, in order to align the interfaces and frame the profiles within each panel. The dashed line shows the initial composition based on Table 2.1.

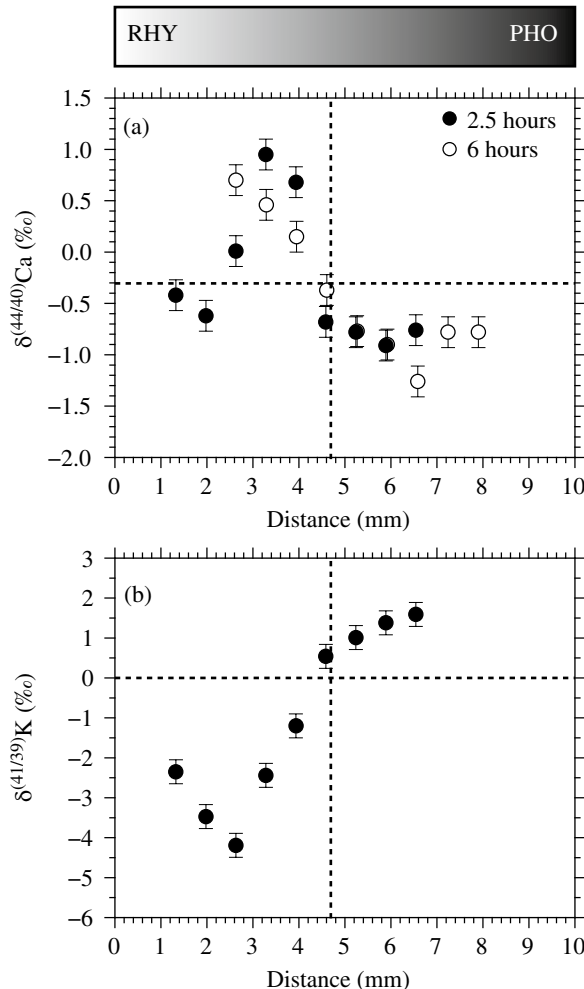


Figure 2.4 Isotopic profiles from two experiments lasting 2.5 hours and 6 hours. Note that the data have been shifted to the right by 1 mm and 2.3 mm for the 2.5 hour and 6 hour runs, respectively, in order to align the interfaces and frame the profiles within each panel.

in the heavy isotope whereas the mafic side is enriched in the light isotope, consistent with a net flux of CaO from the felsic to the mafic liquid despite a negligible initial compositional contrast. In the 2.5-hour run, the $\delta^{44}\text{Ca}$ is equal to the initial value (within error) on the felsic side. It is unclear if the $\delta^{44}\text{Ca}$ has changed from the initial value on the mafic side because the endmost wafer was not successfully extracted during sample preparation. The total range in $\delta^{44}\text{Ca}$ is about 2 in the 2.5-hour run. In the 6-hour run, the shape of the profile is similar but more time-evolved. The Ca isotopic composition has changed significantly from the initial value at both ends of the capsule with a total range in $\delta^{44}\text{Ca}$ of about 1.5‰.

For K isotopes, the shape of the profile resembles those of previous studies where the component of interest diffuses down a monotonic concentration gradient. The net K_2O flux is from phonolite to rhyolite,

which is opposite the CaO flux, rendering the phonolite isotopically heavy and the rhyolite isotopically light. Both ends of the diffusion couple have changed from the initial value because of the fast diffusion of the K_2O component reaching both ends of the capsule. The total range in $\delta^{41}\text{K}$ is about 6‰.

2.4. DISCUSSION

In the first study of its kind on this topic, Richter et al. (1999) performed diffusion couple experiments in the simplified $\text{CaO}-\text{Al}_2\text{O}_3-\text{SiO}_2$ system and developed a theoretical framework whereby the magnitude of diffusive isotopic fractionations correlates positively with the initial concentration contrast between starting materials and the mass dependence on diffusivity. The results presented here, however, show that large diffusive isotope effects can arise even when the initial concentration contrast is very small, as is the case for CaO. Another peculiarity of this system is the extremely fast diffusion of K_2O , which appears to be largely decoupled from that of SiO_2 . This bears similarities to the behavior of Li_2O in the basalt-rhyolite experiments of Richter et al. (2003), but unlike Li_2O , K_2O is a major component, and because of requirements for mass and charge balance, its diffusion influences the profiles of all the other major elements either by dilution, enrichment, or diffusive coupling. Not only does K_2O diffuse rapidly, but it also exhibits large diffusive isotope effects despite there being only a 2 amu difference between ^{41}K and ^{39}K . In following sections, we adapt an existing framework that enables us to model the SiO_2 , CaO, and K_2O profiles and to quantify the mass dependence on diffusion coefficients in order to place the phonolite-rhyolite results in the context of previous studies.

2.5. MODELING

There are two classes of diffusion models that can explain complicated diffusion behavior in a multicomponent system. The first is a more general multicomponent diffusion model that invokes a matrix of diffusion coefficients (Onsager, 1945). The second is a form of effective binary diffusion model in which components diffuse in response to activity gradients, which in turn are given by the concentration of SiO_2 (Richter, 1993; Zhang, 1993).

2.5.1. General Multicomponent Diffusion

In a multi-component system, the diffusive flux J_i (moles m^{-2}/s) of component i is given by:

$$J_i = - \sum_{k=1}^{N-1} D_{ik} \nabla C_k, \quad (2.3)$$

where D_{ik} (m^2/s) is the multicomponent diffusion matrix and C_k is the concentration of component k in volume-normalized units. The off-diagonal terms in the diffusion matrix represent diffusive coupling between components, which may be kinetic (the diffusing species have a stoichiometry that differs from the stoichiometry of the chosen components of the system) or thermodynamic (the flux of one component influences the activity or concentration of another). The full diffusion matrix has been determined for only a few simplified silicate liquid systems (Chakraborty et al., 1995; Kress & Ghiorso, 1993; Liang, 2010; Liang & Davis, 2002; Liang et al., 1996; Mungall et al., 1998; Oishi et al., 1982; Richter et al., 1998; Sugawara et al., 1977; Wakabayashi & Oishi, 1978; Watkins et al., 2014) as well as some basaltic liquids (Guo & Zhang, 2016, 2018; Kress & Ghiorso, 1995). The full diffusion matrix is not known for either phonolite or rhyolite. Even if it were known, it would be composition dependent in the mixing region between the two liquids, and at present there is no general way of dealing with such a complex diffusion problem. Therefore, it is not practical to use a multicomponent diffusion model for describing the fluxes in the rhyolite-phonolite diffusion couple, and a simplified approach must be employed.

2.5.2. The Zhang (1993) Modified Effective Binary Diffusion Model

The effective binary diffusion (EBD) model (Cooper, 1968) is often used in applications where the goal is to infer timescales of magmatic processes in complex systems (cf. Zhang, 2010). In this framework, the flux of component i is proportional to its own concentration gradient:

$$J_i = -D_i^{\text{EBD}} \nabla C_i, \quad (2.4)$$

where D_i^{EBD} is the effective binary diffusion coefficient (EBDC) and is sensitive to melt composition and the direction of diffusion in composition space (Liang, 2010; Zhang, 2010).

There are a number of shortcomings of the EBD model, but the main one for our purposes is that it cannot describe uphill diffusion. This led Zhang (1993) to propose a modified EBD model based on the concept of elemental partitioning between two liquids of different composition. The Zhang model treats the diffusive flux of a component as being proportional to an activity gradient instead of a concentration gradient (following Zhang's notation, we drop the subscript i to make the expressions easier to read):

$$J \approx -\mathcal{D} \frac{\nabla(\gamma C)}{\gamma}, \quad (2.5)$$

where γ is the activity coefficient and \mathcal{D} is the “intrinsic effective binary diffusivity.” At equilibrium, the activity ($a = \gamma C$) is uniform but there may still be concentration gradients, as would be the case for the interface between two phases or two immiscible liquids. Note that $\mathcal{D} = D_i^{\text{EBD}}$ when γ is constant. For simplicity, we adopt the simplest version of the Zhang model and assume that $1/\gamma$ is a linear function of SiO_2 concentration and is independent of the concentration of all other components. Alternatively, one might assume that the activity has an exponential dependence on SiO_2 concentration (e.g., Richter, 1993), but this ultimately yields similar profiles and does not change our overall conclusions (see Supplemental Information 2.A). Regardless, for a given transient profile of SiO_2 , there exists an associated hypothetical “quasi-equilibrium” profile for the equilibrium concentration of the component of interest, C_e , that scales with $1/\gamma$ as well as the concentration of SiO_2 . Assuming that diffusion of SiO_2 can be characterized by a concentration-independent EBD, D_b , and that diffusion of SiO_2 does not reach either end of the diffusion couple, the “equilibrium” concentration profile for C_e is an error function:

$$C_e = \frac{C_- + C_+}{2} + C_f \operatorname{erf} \frac{x}{2\sqrt{D_b t}}, \quad (2.6)$$

where C_- and C_+ are the initial concentrations at $x < 0$ and $x > 0$ for the diffusion couple and C_f is the difference in the equilibrium concentration between the two liquids, as depicted in Fig. 2.5. The parameter C_f can be positive or negative, depending on whether the component preferentially partitions into the high-silica or low-silica liquid. A large C_f implies strong preference for one liquid versus the other. If $C_f = 0$, the model reverts back to the simplified EBD model. Replacing γ with $1/C_e$ in equation 2.5 yields

$$J = -\mathcal{D} C_e \nabla(C/C_e), \quad (2.7)$$

which leads to the one-dimensional diffusion equation (Eq. 9a in Zhang, 1993):

$$\frac{\partial C}{\partial t} = \frac{\partial}{\partial x} \left(\frac{\mathcal{D}}{C_e} \frac{\partial(C/C_e)}{\partial x} \right), \quad (2.8)$$

where the units of concentration may be in weight percent if density can be assumed to be constant. The reason for the approximation symbol in equation 2.5 is that Zhang (1993) uses equation 2.8 to calculate concentration profiles and then calculates activity profiles from the relation $a = kC/C_e$, where k is the proportionality constant

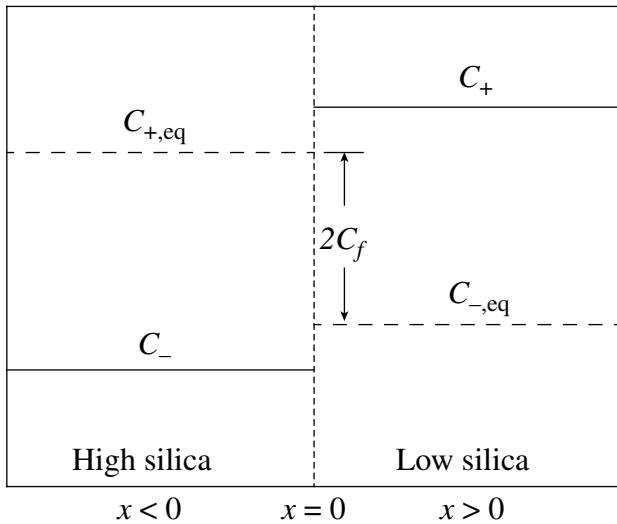


Figure 2.5 The Zhang model and its parameters are based on the concept of elemental partitioning in an SiO_2 gradient. The initial concentration distribution is C_+ for $x > 0$ and C_- for $x < 0$. At equilibrium, the concentration contrast may be reversed (depending on the sign of C_f) such that $C_{+,eq}$ for $x < 0$ and $C_{-,eq}$ for $x > 0$.

between C_e and $1/\gamma$. A point that was nuanced by Zhang (1993) is that equations 2.5 and 2.7 are not equivalent, but rather are scaled by a factor k , which can be determined from the constraint that $a = C$ at $x = 0$ (interface).

Model Validation and Behavior

The Zhang (1993) model deviates significantly from the EBD model when the component of interest diffuses significantly faster than SiO_2 . In this situation, which is common in silicate liquids, the component of interest will not reach homogeneity quickly, but rather, will partition along the compositional continuum between the high- and low-silica liquids and reach compositional homogeneity only as fast as SiO_2 diffuses.

The behavior of the model is shown in Fig. 2.6 for an infinite diffusion couple where the initial concentration gradient is small and $D/D_b = 8$. If C_f is negative (Fig. 2.6a), the element partitions into the high-silica liquid and the hypothetical C_e gradient opposes the concentration gradient. In this case, mass diffuses from the high concentration to the low concentration side at a higher rate than if $C_f=0$, resulting in a pair of bumps in the concentration profile. If C_f is positive (Fig. 2.6b), the activity gradient is opposite the concentration gradient and uphill diffusion occurs. Note that in both cases, the C_e profile evolves at a rate given by D_b (equation 2.6) and is thus less evolved than the concentration profiles exhibiting uphill diffusion.

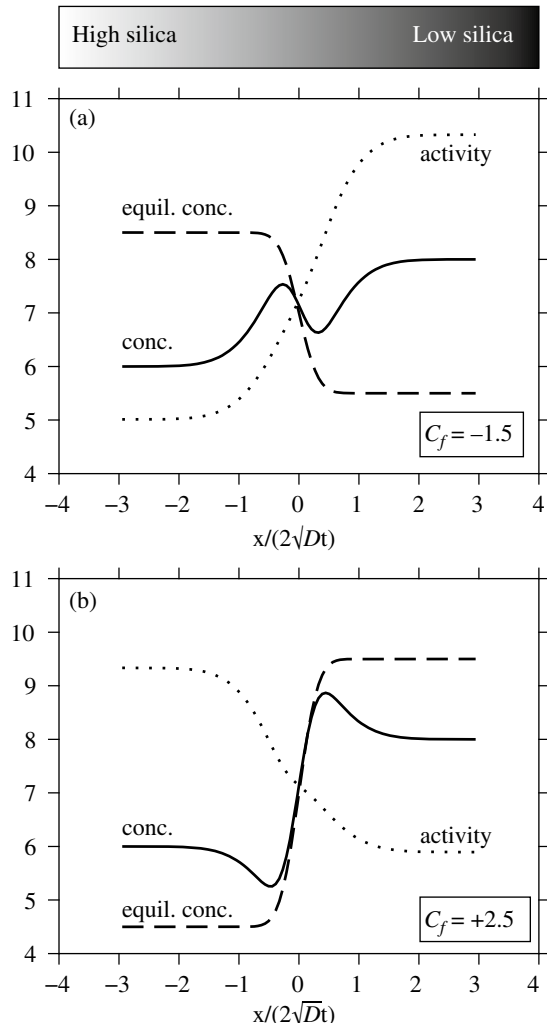


Figure 2.6 Model behavior showing concentration, activity, and transient equilibrium concentration profiles for $C_- = 6 \text{ wt\%}$, $C_+ = 8 \text{ wt\%}$, $D/D_b = 8$, and variable C_f . The top panel is identical to Fig. 2c in Zhang (1993) to validate the Matlab code used in calculations herein. For an element with small initial concentration contrast, the sign and magnitude of uphill diffusion depends on the sign and magnitude of C_f , which describes how the element partitions between high silica versus low silica liquids.

Model Applied to the Rhyolite-Phonolite Couples

The rhyolite-phonolite diffusion couple spans a broad range of melt compositions. Although the diffusion coefficients are expected to be sensitive to melt composition across this range, we assume D and D_b are constant. We also treat the diffusion couple as infinite with respect to SiO_2 even though we see some uphill diffusion of SiO_2 at the ends of the couple in the 2.5 hour run. This, however, may just be due to mass balance and dilution effects caused by the faster diffusing components. For the faster diffusing K_2O and CaO components, the diffusion couple is not treated as infinite; i.e., $\partial C/\partial x = 0$ at the boundaries.

Despite the many simplifying assumptions that are needed to distill a general multicomponent diffusion problem down to a three-parameter model (C_f , D_b , and \mathcal{D}), the modified EBD model is capable of reproducing the sign and magnitude of uphill diffusion in the K_2O and CaO profiles (Fig. 2.7a–f). The positive C_f for CaO implies that CaO partitions into mafic liquids whereas the negative C_f for K_2O implies that K_2O partitions into felsic liquids, which is consistent with the known partitioning behavior of these two oxide components (Ryerson & Hess, 1978; Watson, 1976). The misfit on the ends of the CaO profiles suggest that the activity of CaO depends on melt components in addition to SiO_2 . The next level of complexity would be to include the alkali components in the activity-composition model for CaO .

The goodness-of-fit for the K_2O profile is even less satisfying due to the unusual shape of the measured K_2O

profile, which is nearly flat on the mafic side and linear to nearly convex on the felsic side. This shape cannot be reproduced using the simplified EBD models discussed herein. Nevertheless, the inferred \mathcal{D}_{K_2O} is a reasonable average value, being somewhat overestimated on the rhyolite side and somewhat underestimated on the phonolite side. A better fit could be obtained by casting \mathcal{D}_{K_2O} as a function of SiO_2 concentration (Richter et al., 2003, 2009; Watkins et al., 2009) or by introducing some other additional ad hoc complexity into the model. We did not undertake such efforts because the calculated concentration profiles provide an adequate description of the K_2O fluxes to be used as a baseline for modeling the isotope ratio profiles.

Model for the Isotope Ratio Profiles

Model isotope ratio profiles are generated by invoking a difference in diffusivity between the isotopes of an

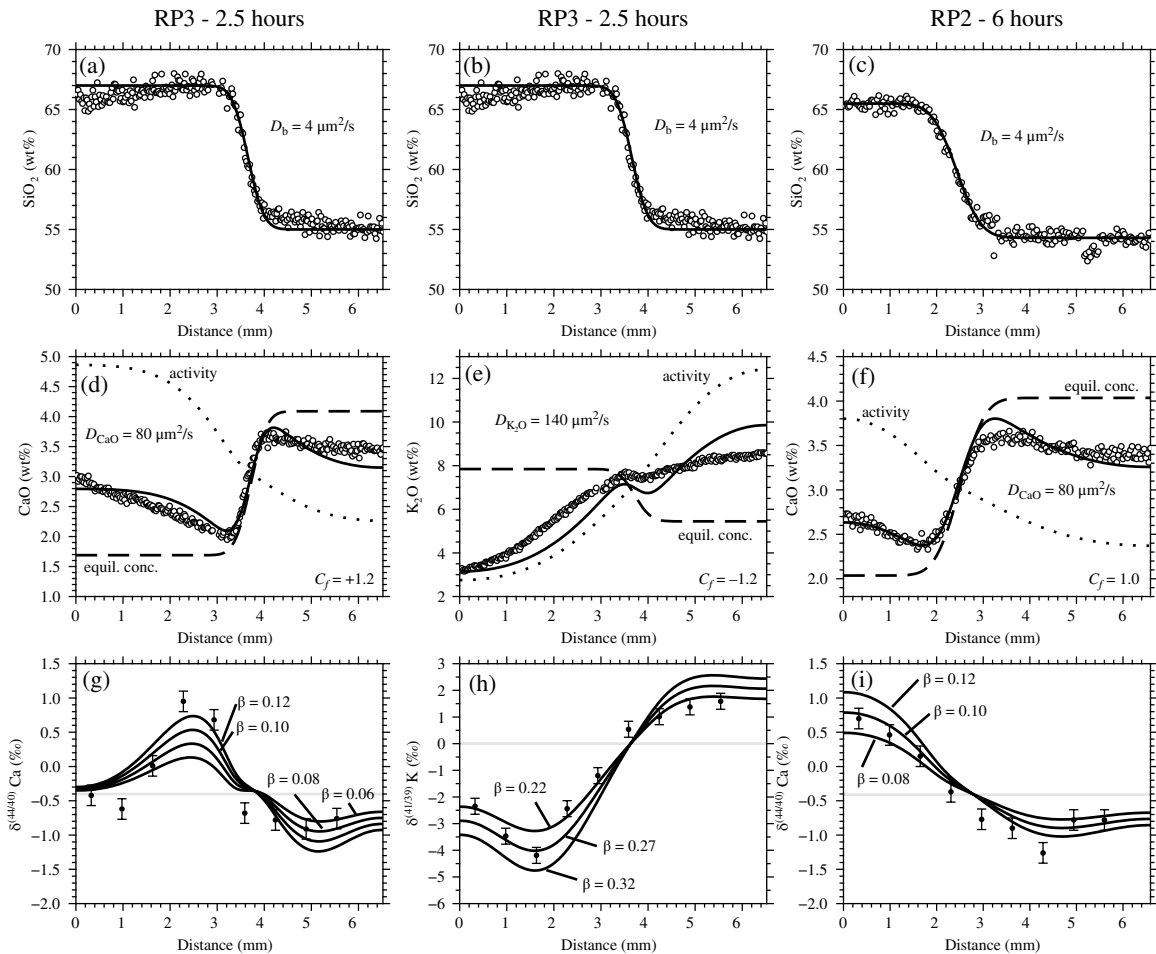


Figure 2.7 The modified EBD model applied to the data. Top panels: SiO_2 diffusion is well-approximated as effective binary in an infinite medium. Middle panels: Both CaO and K_2O exhibit uphill diffusion, which is attributed in the model to transient partitioning between high-silica and low-silica liquids. Bottom panels: Despite the simplifying assumptions, the model captures the sign and magnitude of diffusive isotope effects.

element. The dependence of diffusivity on mass can be written as (Richter et al., 1999):

$$\frac{D_{44}}{D_{40}} = \left(\frac{m_{40}}{m_{44}} \right)^\beta \approx \left(\frac{40}{44} \right)^\beta, \quad (2.9)$$

where β is a dimensionless empirical parameter. Here, m refers to the isotopic mass and not the mass of an isotopically substituted molecule such as, for example, CaAl_2O_4 . This functional form is based on principles from the kinetic theory of gases, but it's also convenient because it normalizes out the fractional mass difference between isotopes, thereby allowing for direct comparison between different isotopic systems.

To model the isotope ratio profiles, we assume the rhyolite and phonolite have the same isotopic composition since they are within error of each other with respect to $\delta^{44}\text{Ca}$. Although we did not directly measure the $\delta^{41}\text{K}$ of either starting material, the assumption that they are the same can be justified on the basis that the global range in $\delta^{41}\text{K}$ of igneous rocks and minerals is $< 1\text{\textperthousand}$ (Morgan et al., 2018). We assume further that the equilibrium isotope ratio profile is uniform at all times; i.e., $C_{e,44}$ is defined to be proportional to $C_{e,40}$ such that the ratio $C_{e,44}/C_{e,40}$ is constant, which implies that there is no equilibrium isotopic partitioning between the liquids. Hence, any isotopic fractionations in the model arise solely from diffusive fluxes and the difference in isotopic diffusion coefficients.

Model isotopic profiles are compared to the data in the bottom panels of Fig. 2.7. For Ca isotopes, no single set of parameters (D_{CaO} , D_b , C_f , and β) can explain the full profile or its time evolution reflected in the 2.5- and 6-hour runs. Nevertheless, the fits are qualitatively no worse than those used to estimate β factors and associated uncertainties in other natural silicate liquid diffusion couple experiments (Richter et al., 2003; Watkins et al., 2009). By plotting model curves corresponding to different values of β against the data, we estimate $\beta = 0.10 \pm 0.02$. This is a somewhat crude estimate, however, and appears to be on the low side for the rhyolite while fitting the phonolite in the 2.5-hour run, and on the low side for the phonolite while fitting the rhyolite in the 6-hour run. For K isotopes, we estimate $\beta = 0.25 \pm 0.03$, which is comparable to the value for Li ($\beta = 0.21\text{--}0.23$) in basalt-rhyolite and rhyolite-rhyolite diffusion couples (Holycross et al., 2018; Richter et al., 2003).

2.5.3. Comparison to Previous Studies

It was shown previously that β factors correlate with the diffusivity of the cation normalized by that of Si (or SiO_2) (Fig. 2.8). Since Si is strongly bound in multi-atom

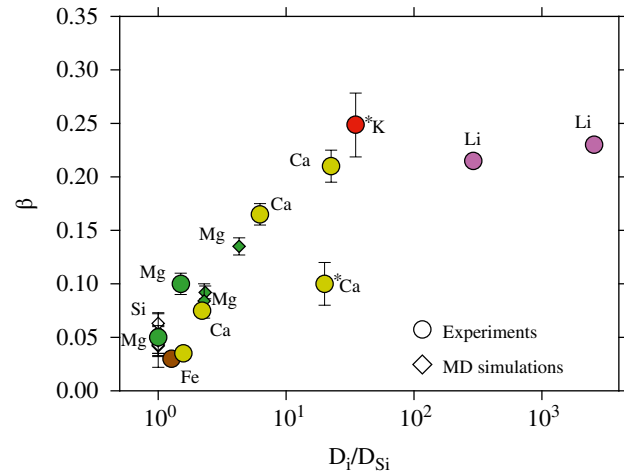


Figure 2.8 β factors from this study (points with an asterisk) compared to literature values. The quantity $D_{\text{CaO}}/D_{\text{Si}}$ is used as a proxy for extent to which a diffusing cation is coupled to the melt matrix. The Ca β factor is offset from the overall trend, but this may be because D_{CaO} is overestimated. The β factor for K is the largest value yet reported for diffusion in silicate liquids.

complexes with O (as well as Al and other Si atoms), it diffuses more slowly than other elements, and hence the ratio D/D_{Si} is generally greater than unity. For elements present in major quantities, the ratio D/D_{Si} is typically close to unity because of the cooperative motion that is required to yield a net flux of counter-diffusing major elements. The regime where D/D_{Si} is high tends to occur in more silica-rich liquids and with decreasing temperature (Dingwell, 1990).

The ratio $D_{\text{CaO}}/D_{\text{Si}}$ is inferred to be about 20, and the β factor for Ca is offset from the overall trend. The ratio $D_{\text{K}_2\text{O}}/D_{\text{Si}}$ is inferred to be about 35 and the β factor for K is the highest value yet determined for diffusion in silicate liquids. Despite K_2O being present in major quantities, it behaves like a trace element insofar as its diffusion is kinetically decoupled from the motion of the slower-moving aluminosilicate structures (cf. Dingwell, 1990). The high β factor suggests that large diffusive isotope effects can arise in high- T environments and our results should aid in the search for, and interpretation of, potentially large kinetic K isotope effects in nature.

2.6. CONCLUSIONS AND POSSIBLE FUTURE APPLICATIONS

We performed a set of diffusion couple experiments involving unusual phonolite and rhyolite compositions. The data and analysis of those experiments presented

here provides additional β factors needed for modeling reaction and transport processes in high temperature geologic systems. Despite the complicated nature of the diffusion profiles, which is an inevitability when dealing with natural silicate liquid compositions, we showed how one can extract a meaningful β factor from the diffusion profiles using a modified effective binary diffusion model that was first developed by Zhang (1993). Our results confirm that β factors vary depending on the element as well as liquid composition, and also that large diffusive isotope effects can arise even in the absence of a large initial concentration gradient. The retrieved β factor for Ca is typical of Ca in natural silicate liquids whereas the β factor for K is the highest value yet reported, suggesting that large diffusive K isotope effects may yet be found in high- T environments.

One of the goals of this type of experimental study is to use the growing compilation of β factors to better understand how the mobility of key chemical constituents is controlled, and how that mobility relates to isotopic fractionation of Ca, Mg, Fe, Si, and K in high temperature systems. Recent work shows how isotopic effects in these elements can be used as tracers of micro- and nano-scale processes at mineral surfaces and transport within geologic media at larger scales. For example, Antonelli et al. (2019a) documented small Ca isotope fractionations between volcanic phenocrysts (plagioclase, clinopyroxene, hornblende, and olivine) of various sizes (mm to cm) in lavas ranging in composition from alkali basalt to rhyodacite. They interpreted the effects as being due to diffusive isotope fractionation during crystal growth superimposed on small equilibrium fractionation effects. With knowledge of β factors, they used the model of Watson and Müller (2009) to show how Ca isotope fractionation could be used as a measure of crystal growth rates. They inferred plagioclase growth rates of order 0.03 to 0.3 cm/yr, which is in broad agreement with other estimates of typical volcanic phenocryst growth rates. This approach can be extended to other K-bearing minerals (e.g., K-spar, muscovite) using K isotopes in lieu of Ca isotopes.

Another example is the study by Chopra et al. (2012), who used their knowledge of Mg isotope fractionation effects to evaluate the isotopic gradients at the boundaries of a pillowed mafic dike intruded into a granitic intrusion at Vinalhaven, Maine. They used the isotope effects to confirm that diffusion was responsible for the chemical gradients and estimated a diffusion timescale for cooling of the dike-granite system. We envision extending this to other elements (Ca and K) and other sites. There are many field localities where a mafic (gabbroic) magma with 6–8% CaO and < 1% K₂O has

intruded a more silicic (granitic) body with 1–2% CaO and 2–5% K₂O. The Ca concentration gradient is downward toward the granitic phase and the K concentration gradient is downward toward the gabbroic phase. We anticipate that the use of two or more isotopic systems, such as Ca and K, with different temperature-dependent diffusivities could provide unique information on mixing and cooling processes in magmatic systems.

APPENDIX LINEAR VERSUS EXPONENTIAL DEPENDENCE OF ACTIVITY ON SiO₂

Here we show that the model outputs and conclusions are not dependent on whether the activity is linearly or exponentially dependent on SiO₂ concentration. If the activity is an exponential function of SiO₂, then the equation for C_e

$$C_e = \frac{C_- + C_+}{2} + C_f \operatorname{erf} \frac{x}{2\sqrt{D_b t}}, \quad (2.A1)$$

becomes

$$C_e = \frac{C_- + C_+}{2} e^{\frac{B \cdot \operatorname{erf} \frac{x}{2\sqrt{D_b t}}}{2}}, \quad (2.A2)$$

where the parameter B is functionally similar to the parameter C_f (Zhang, 1993). An exponential dependence was also adopted by Richter (1993). Fig. 2.9 compares the two approaches side by side and shows that the results and conclusions are not sensitive to this particular aspect of the Zhang model.

ACKNOWLEDGMENTS

We are grateful for constructive reviews by James Van Orman and an anonymous reviewer. The experimental work of JMW was supported primarily by the National Science Foundation under Grant Nos. EAR0838168 and EAR0608885 to DJD. Support for isotopic analysis was also provided by the Director, Office of Science, Office of Basic Energy Sciences, of the U.S. Department of Energy under Contract No. DEAC02-05CH11231. This work was partially performed under the auspices of the U.S. Department of Energy by the University of California, Lawrence Livermore National Laboratory, under Contract Nos. W-7405-Eng-48, DE-AC52-07NA27344, and DE-AC02-05CH1123.

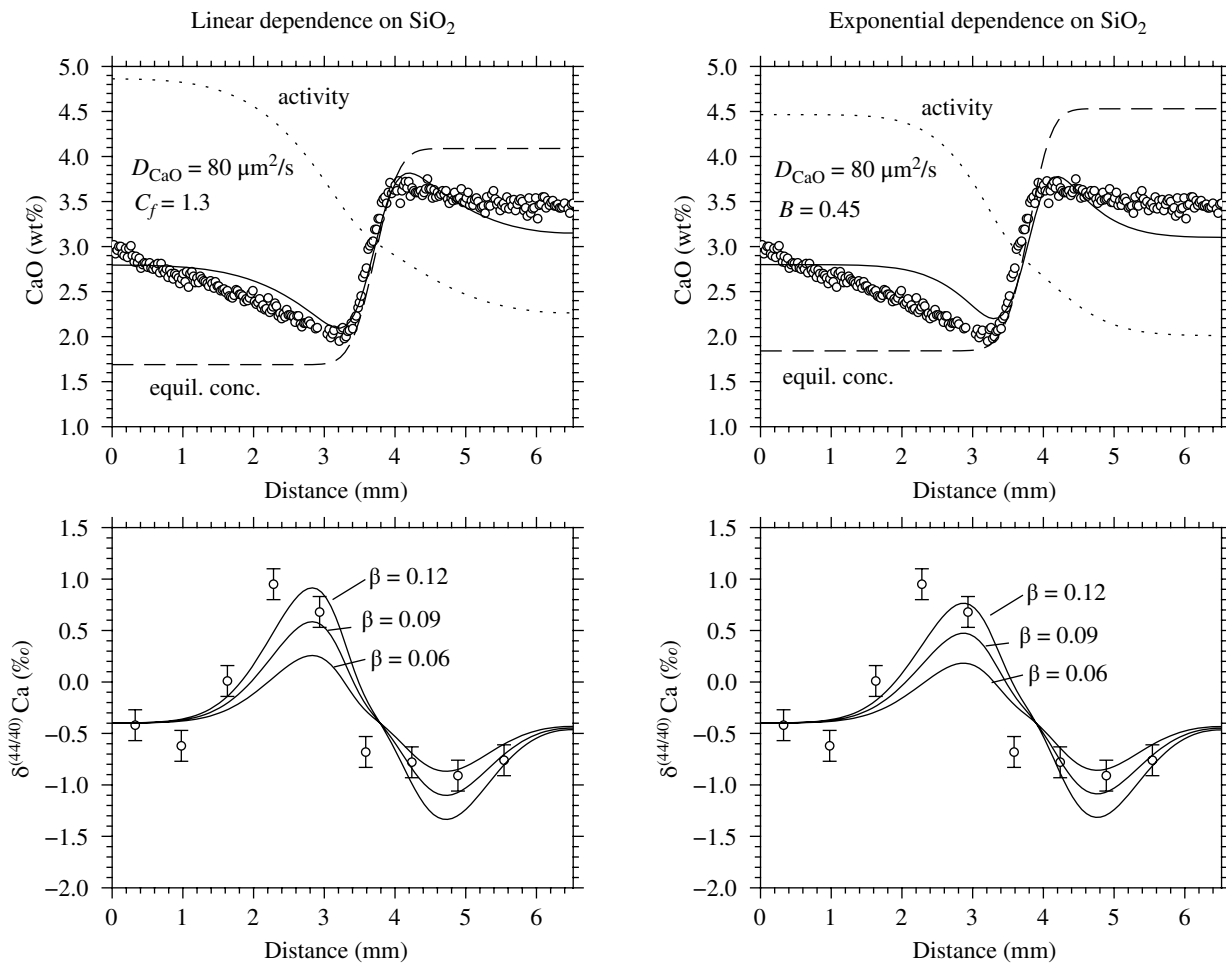


Figure 2.9 The 2.5 hour run modeled using a linear dependence of CaO activity on SiO_2 (left panels) versus and exponential dependence on SiO_2 (right panels). The inferred β factors are the same regardless of which approach is used.

REFERENCES

- Antonelli, M., Mittal, T., McCarthy, A., Tripoli, B., Watkins, J., & DePaolo, D. (2019a). Ca isotopes record rapid crystal growth in volcanic and subvolcanic systems. *Proceedings of the National Academy of Sciences*, 116, 20315–20321. <https://doi.org/10.1073/pnas.1908921116>
- Antonelli, M. A., Schiller, M., Schauble, E. A., Mittal, T., DePaolo, D. J., Chacko, T., et al. (2019b). Kinetic and equilibrium Ca isotope effects in high-T rocks and minerals. *Earth and Planetary Science Letters*, 517, 71–82. <https://doi.org/10.1016/j.epsl.2019.04.013>
- Barrat, J.-A., Chaussidon, M., Bohn, M., Gillet, P., Göpel, C., & Lesourd, M. (2005). Lithium behavior during cooling of a dry basalt: An ion-microprobe study of the lunar meteorite Northwest Africa 479 (NWA 479). *Geochimica et Cosmochimica Acta*, 69(23), 5597–5609. <https://doi.org/10.1016/j.gca.2005.06.032>
- Beck, P., Chaussidon, M., Barrat, J.-A., Gillet, P., & Bohn, M. (2006). Diffusion induced Li isotopic fractionation during the cooling of magmatic rocks: the case of pyroxene phenocrysts from nakhlite meteorites. *Geochimica et Cosmochimica Acta*, 70(18), 4813–4825. <https://doi.org/10.1016/j.gca.2006.07.025>
- Bourg, I. C., Richter, F. M., Christensen, J. N., & Sposito, G. (2010). Isotopic mass dependence of metal cation diffusion coefficients in liquid water. *Geochimica et Cosmochimica Acta*, 74(8), 2249–2256. <https://doi.org/10.1016/j.gca.2010.01.024>
- Chakraborty, S., Dingwell, D. B., & Rubie, D. C. (1995). Multicomponent diffusion in ternary silicate melts in the system $\text{K}_2\text{O}-\text{Al}_2\text{O}_3-\text{SiO}_2$: II. Mechanisms, systematics, and geological applications. *Geochimica et Cosmochimica Acta*, 59(2), 265–277. [https://doi.org/10.1016/0016-7037\(94\)00283-R](https://doi.org/10.1016/0016-7037(94)00283-R)
- Chen, L.-M., Teng, F.-Z., Song, X.-Y., Hu, R.-Z., Yu, S.-Y., Zhu, D., & Kang, J. (2018). Magnesium isotopic evidence for chemical disequilibrium among cumulus minerals in layered

- mafic intrusion. *Earth and Planetary Science Letters*, 487, 74–83. <https://doi.org/10.1016/j.epsl.2018.01.036>
- Chopra, R., Richter, F. M., Watson, E. B., & Scullard, C. R. (2012). Magnesium isotope fractionation by chemical diffusion in natural settings and in laboratory analogues. *Geochimica et Cosmochimica Acta*, 88, 1–18. <https://doi.org/10.1016/j.gca.2012.03.039>
- Christensen, J. N., Qin, L., Brown, S. T., & DePaolo, D. J. (2018). Potassium and calcium isotopic fractionation by plants (soybean [*Glycine max*], rice [*Oryza sativa*], and wheat [*Triticum aestivum*]). *ACS Earth and Space Chemistry*, 2(7), 745–752. <https://doi.org/10.1021/acsearthspacechem.8b00035>
- Cooper, A. R. (1968). The use and limitations of the concept of an effective binary diffusion coefficient for multi-component diffusion. *Mass Transport in Oxides*, 296, 79–84.
- Dauphas, N. (2007). Diffusion-driven kinetic isotope effect of Fe and Ni during formation of the Widmanstätten pattern. *Meteoritics & Planetary Science*, 42(9), 1597–1613. <https://doi.org/10.1111/j.1945-5100.2007.tb00593.x>
- Dauphas, N., Teng, F.-Z., & Arndt, N. T. (2010). Magnesium and iron isotopes in 2.7 Ga Alexo komatiites: mantle signatures, no evidence for Soret diffusion, and identification of diffusive transport in zoned olivine. *Geochimica et Cosmochimica Acta*, 74(11), 3274–3291. <https://doi.org/10.1016/j.gca.2010.02.031>
- Dingwell, D. B. (1990). Effects of structural relaxation on cationic tracer diffusion in silicate melts. *Chemical Geology*, 82, 209–216. [https://doi.org/10.1016/0009-2541\(90\)90082-I](https://doi.org/10.1016/0009-2541(90)90082-I)
- Gallagher, K., & Elliott, T. (2009). Fractionation of lithium isotopes in magmatic systems as a natural consequence of cooling. *Earth and Planetary Science Letters*, 278(3–4), 286–296. <https://doi.org/10.1016/j.epsl.2008.12.009>
- Gao, Y., Snow, J. E., Casey, J. F., & Yu, J. (2011). Cooling-induced fractionation of mantle Li isotopes from the ultraslow-spreading Gakkel Ridge. *Earth and Planetary Science Letters*, 301(1–2), 231–240. <https://doi.org/10.1016/j.epsl.2010.11.003>
- Goel, G., Zhang, L., Lacks, D. J., & Van Orman, J. A. (2012). Isotope fractionation by diffusion in silicate melts: Insights from molecular dynamics simulations. *Geochimica et Cosmochimica Acta*, 93, 205–213. <https://doi.org/10.1016/j.gca.2012.07.008>
- Guo, C., & Zhang, Y. (2016). Multicomponent diffusion in silicate melts: $\text{SiO}_2\text{-TiO}_2\text{-Al}_2\text{O}_5\text{-MgO}\text{-CaO}\text{-Na}_2\text{O}\text{-K}_2\text{O}$ system. *Geochimica et Cosmochimica Acta*, 195, 126–141. <https://doi.org/10.1016/j.gca.2016.09.003>
- Guo, C., & Zhang, Y. (2018). Multicomponent diffusion in basaltic melts at 1350°C. *Geochimica et Cosmochimica Acta*, 228, 190–204. <https://doi.org/10.1016/j.gca.2018.02.043>
- Holycross, M., Watson, E., Richter, F., & Villeneuve, J. (2018). Diffusive fractionation of Li isotopes in wet, highly silicic melts. *Geochemical Perspectives Letters*, 6, 39–42. doi: 10.7185/geochemlet.1807
- Jeffcoate, A., Elliott, T., Kasemann, S., Ionov, D., Cooper, K., & Brooker, R. (2007). Li isotope fractionation in peridotites and mafic melts. *Geochimica et Cosmochimica Acta*, 71(1), 202–218. <https://doi.org/10.1016/j.gca.2006.06.1611>
- Kil, Y., Jung, H., & Yang, K. (2016). Li isotopic disequilibrium of the Cenozoic subcontinental lithospheric mantle in East Asia. *Geosciences Journal*, 20(5), 597–607. <https://doi.org/10.1007/s12303-016-0024-y>
- Kress, V., & Ghiorso, M. (1993). Multicomponent diffusion in $\text{MgO}\text{-Al}_2\text{O}_3\text{-SiO}_2$ and $\text{CaO}\text{-MgO}\text{-Al}_2\text{O}_3\text{-SiO}_2$ melts. *Geochimica et Cosmochimica Acta*, 57(18), 4453–4466. [https://doi.org/10.1016/0016-7037\(93\)90495-I](https://doi.org/10.1016/0016-7037(93)90495-I)
- Kress, V. C., & Ghiorso, M. S. (1995). Multicomponent diffusion in basaltic melts. *Geochimica et Cosmochimica Acta*, 59(2), 313–324. [https://doi.org/10.1016/0016-7037\(94\)00286-U](https://doi.org/10.1016/0016-7037(94)00286-U)
- Liang, Y. (2010). Multicomponent diffusion in molten silicates: theory, experiments, and geological applications. *Reviews in Mineralogy and Geochemistry*, 72(1), 409–446. <https://doi.org/10.2138/rmg.2010.72.9>
- Liang, Y., & Davis, A. M. (2002). Energetics of multicomponent diffusion in molten $\text{CaO}\text{-Al}_2\text{O}_3\text{-SiO}_2$. *Geochimica et Cosmochimica Acta*, 66(4), 635–646. [https://doi.org/10.1016/S0016-7037\(01\)00793-1](https://doi.org/10.1016/S0016-7037(01)00793-1)
- Liang, Y., Richter, F. M., & Watson, E. B. (1996). Diffusion in silicate melts: II. Multicomponent diffusion in $\text{CaO}\text{-Al}_2\text{O}_3\text{-SiO}_2$ at 1500 °C and 1 GPa. *Geochimica et Cosmochimica Acta*, 60(24), 5021–5035. [https://doi.org/10.1016/S0016-7037\(96\)00352-3](https://doi.org/10.1016/S0016-7037(96)00352-3)
- Lundstrom, C. C., Chaussidon, M., Hsui, A. T., Kelemen, P., & Zimmerman, M. (2005). Observations of Li isotopic variations in the Trinity Ophiolite: evidence for isotopic fractionation by diffusion during mantle melting. *Geochimica et Cosmochimica Acta*, 69(3), 735–751. <https://doi.org/10.1016/j.gca.2004.08.004>
- Marschall, H. R., von Strandmann, P. A. P., Seitz, H.-M., Elliott, T., & Niu, Y. (2007). The lithium isotopic composition of orogenic eclogites and deep subducted slabs. *Earth and Planetary Science Letters*, 262(3–4), 563–580. doi: 10.1016/j.epsl.2007.08.005
- Morgan, L. E., Ramos, D. P. S., Davidheiser-Kroll, B., Faithfull, J., Lloyd, N. S., Ellam, R. M., & Higgins, J. A. (2018). High-precision $^{41}\text{K}/^{39}\text{K}$ measurements by MC-ICP-MS indicate terrestrial variability of $\delta^{41}\text{K}$. *Journal of Analytical Atomic Spectrometry*, 33(2), 175–186. <https://doi.org/10.1039/C7JA00257B>
- Mueller, T., Watson, E. B., Trail, D., Wiedenbeck, M., Van Orman, J., & Hauri, E. H. (2014). Diffusive fractionation of carbon isotopes in γ -Fe: Experiment, models and implications for early solar system processes. *Geochimica et Cosmochimica Acta*, 127, 57–66. <https://doi.org/10.1016/j.gca.2013.11.014>
- Mungall, J. E., Romano, C., & Dingwell, D. B. (1998). Multicomponent diffusion in the molten system $\text{K}_2\text{O}\text{-Na}_2\text{O}\text{-Al}_2\text{O}_3\text{-SiO}_2\text{-H}_2\text{O}$. *American Mineralogist*, 83(7–8), 685–699. <https://doi.org/10.2138/am-1998-7-802>
- Oeser, M., Dohmen, R., Horn, I., Schuth, S., & Weyer, S. (2015). Processes and time scales of magmatic evolution as revealed by Fe–Mg chemical and isotopic zoning in natural olivines. *Geochimica et Cosmochimica Acta*, 154, 130–150. <https://doi.org/10.1016/j.gca.2015.01.025>
- Oishi, Y., Nanba, M., & Pask, J. A. (1982). Analysis of liquid-state interdiffusion in the system $\text{CaO}\text{-Al}_2\text{O}_3\text{-SiO}_2$ using multiaionic ion models. *Journal of the American Ceramic Society*, 65(5), 247–253. doi: 10.1111/j.1151-2916.1982.tb10427.x
- Onsager, L. (1945). Theories and problems of liquid diffusion. *Annals of the New York Academy of Sciences*, 46(5), 241–265. <https://doi.org/10.1111/j.1749-6632.1945.tb36170.x>

- Parkinson, I. J., Hammond, S. J., James, R. H., & Rogers, N. W. (2007). High-temperature lithium isotope fractionation: Insights from lithium isotope diffusion in magmatic systems. *Earth and Planetary Science Letters*, 257(3–4), 609–621. doi: 10.1016/j.epsl.2007.03.023
- Richter, F. M. (1993). A method for determining activity-composition relations using chemical diffusion in silicate melts. *Geochimica et Cosmochimica Acta*, 57(9), 2019–2032. https://doi.org/10.1016/0016-7037(93)90090-J
- Richter, F., Chaussidon, M., Mandybaev, R., & Kite, E. (2016). Reassessing the cooling rate and geologic setting of Martian meteorites MIL 03346 and NWA 817. *Geochimica et Cosmochimica Acta*, 182, 1–23. https://doi.org/10.1016/j.gca.2016.02.020
- Richter, F., Chaussidon, M., Watson, E. B., Mandybaev, R., & Homolova, V. (2017). Lithium isotope fractionation by diffusion in minerals Part 2: Olivine. *Geochimica et Cosmochimica Acta*, 219, 124–142. https://doi.org/10.1016/j.gca.2017.09.001
- Richter, F. M., Davis, A. M., DePaolo, D. J., & Watson, E. B. (2003). Isotope fractionation by chemical diffusion between molten basalt and rhyolite. *Geochimica et Cosmochimica Acta*, 67(20), 3905–3923. https://doi.org/10.1016/S0016-7037(03)00174-1
- Richter, F. M., Liang, Y., & Davis, A. M. (1999). Isotope fractionation by diffusion in molten oxides. *Geochimica et Cosmochimica Acta*, 63(18), 2853–2861. https://doi.org/10.1016/S0016-7037(99)00164-7
- Richter, F. M., Liang, Y., & Minarik, W. G. (1998). Multicomponent diffusion and convection in molten $MgO\text{-Al}_2\text{O}_3\text{-SiO}_2$. *Geochimica et Cosmochimica Acta*, 62(11), 1985–1991. https://doi.org/10.1016/S0016-7037(98)00123-9
- Richter, F. M., Mandybaev, R. A., Christensen, J. N., Ebel, D., & Gaffney, A. (2011). Laboratory experiments bearing on the origin and evolution of olivine-rich chondrules. *Meteoritics & Planetary Science*, 46(8), 1152–1178. https://doi.org/10.1111/j.1945-5100.2011.01220.x
- Richter, F., Watson, B., Chaussidon, M., Mandybaev, R., & Rusutto, D. (2014). Lithium isotope fractionation by diffusion in minerals. Part 1: Pyroxenes. *Geochimica et Cosmochimica Acta*, 126, 352–370. https://doi.org/10.1016/j.gca.2013.11.008
- Richter, F. M., Watson, E. B., Mandybaev, R., Dauphas, N., Georg, B., Watkins, J., & Valley, J. (2009). Isotopic fractionation of the major elements of molten basalt by chemical and thermal diffusion. *Geochimica et Cosmochimica Acta*, 73(14), 4250–4263. https://doi.org/10.1016/j.gca.2009.04.011
- Roskosz, M., Luais, B., Watson, H. C., Toplis, M. J., Alexander, C. M., & Mysen, B. O. (2006). Experimental quantification of the fractionation of Fe isotopes during metal segregation from a silicate melt. *Earth and Planetary Science Letters*, 248(3), 851–867. doi: 10.1016/j.epsl.2006.06.037
- Rudnick, R. L., & Ionov, D. A. (2007). Lithium elemental and isotopic disequilibrium in minerals from peridotite xenoliths from far-east Russia: product of recent melt/fluid–rock reaction. *Earth and Planetary Science Letters*, 256(1–2), 278–293. https://doi.org/10.1016/j.epsl.2007.01.035
- Ryerson, F., Hess, P. (1978). Implications of liquid-liquid distribution coefficients to mineral-liquid partitioning. *Geochimica et Cosmochimica Acta*, 42(6), 921–932. https://doi.org/10.1016/0016-7037(78)90103-5
- Sio, C. K. I., Dauphas, N., Teng, F.-Z., Chaussidon, M., Helz, R. T., & Roskosz, M. (2013). Discerning crystal growth from diffusion profiles in zoned olivine by in situ Mg–Fe isotopic analyses. *Geochimica et Cosmochimica Acta*, 123, 302–321. https://doi.org/10.1016/j.gca.2013.06.008
- Skulan, J., DePaolo, D. J., & Owens, T. L. (1997). Biological control of calcium isotopic abundances in the global calcium cycle. *Geochimica et Cosmochimica Acta*, 61(12), 2505–2510. https://doi.org/10.1016/S0016-7037(97)00047-1
- Su, B.-X., Zhou, M.-F., & Robinson, P. T. (2016). Extremely large fractionation of Li isotopes in a chromitite-bearing mantle sequence. *Scientific Reports*, 6, 22370. https://doi.org/10.1038/srep22370
- Sugawara, H., Nagata, K., & Goto, K. (1977). Interdiffusivities matrix of $\text{CaO}\text{-Al}_2\text{O}_3\text{-SiO}_2$ melt at 1723 K to 1823 K. *Metallurgical Transactions B*, 8(3), 605–612. https://doi.org/10.1007/BF02658629
- Teng, F.-Z., Dauphas, N., Helz, R. T., Gao, S., & Huang, S. (2011). Diffusion-driven magnesium and iron isotope fractionation in Hawaiian olivine. *Earth and Planetary Science Letters*, 308(3–4), 317–324. doi: 10.1016/j.epsl.2011.06.003
- Teng, F.-Z., McDonough, W. F., Rudnick, R. L., & Walker, R. J. (2006). Diffusion-driven extreme lithium isotopic fractionation in country rocks of the Tin Mountain pegmatite. *Earth and Planetary Science Letters*, 243(3), 701–710. doi: 10.1016/j.epsl.2006.01.036
- Wakabayashi, H., & Oishi, Y. (1978). Liquid-state diffusion of $\text{Na}_2\text{O}\text{-CaO}\text{-SiO}_2$ system. *The Journal of Chemical Physics*, 68(5), 2046–2052. https://doi.org/10.1063/1.436027
- Watkins, J. M. (2010). *Elemental and isotopic separation by diffusion in geological liquids*. Ph.D. thesis, UC Berkeley.
- Watkins, J. M., DePaolo, D. J., Huber, C., & Ryerson, F. J. (2009). Liquid composition-dependence of calcium isotope fractionation during diffusion in molten silicates. *Geochimica et Cosmochimica Acta*, 73(24), 7341–7359. https://doi.org/10.1016/j.gca.2009.09.004
- Watkins, J. M., DePaolo, D. J., Ryerson, F. J., & Peterson, B. T. (2011). Influence of liquid structure on diffusive isotope separation in molten silicates and aqueous solutions. *Geochimica et Cosmochimica Acta*, 75(11), 3103–3118. https://doi.org/10.1016/j.gca.2011.03.002
- Watkins, J. M., DePaolo, D. J., & Watson, E. B. (2017). Kinetic fractionation of non-traditional stable isotopes by diffusion and crystal growth reactions. *Reviews in Mineralogy and Geochemistry*, 82(1), 85–125. https://doi.org/10.2138/rmg.2017.82.4
- Watkins, J. M., Liang, Y., Richter, F., Ryerson, F. J., & DePaolo, D. J. (2014). Diffusion of multi-isotopic chemical species in molten silicates. *Geochimica et Cosmochimica Acta*, 139, 313–326. https://doi.org/10.1016/j.gca.2014.04.039
- Watson, E. B. (1976). Two-liquid partition coefficients: experimental data and geochemical implications. *Contributions to Mineralogy and Petrology*, 56(1), 119–134. https://doi.org/10.1007/BF00375424
- Watson, E. B., & Müller, T. (2009). Non-equilibrium isotopic and elemental fractionation during diffusion-controlled crystal growth under static and dynamic conditions. *Chemical Geology*, 267(3–4), 111–124. https://doi.org/10.1016/j.chemgeo.2008.10.036

42 ISOTOPIC CONSTRAINTS ON EARTH SYSTEM PROCESSES

- Wu, H., He, Y., Teng, F.-Z., Ke, S., Hou, Z., & Li, S. (2018). Diffusion-driven magnesium and iron isotope fractionation at a gabbro-granite boundary. *Geochimica et Cosmochimica Acta*, 222, 671–684. <https://doi.org/10.1016/j.gca.2017.11.010>
- Yogodzinski, G., Vervoort, J., Brown, S. T., & Gerseny, M. (2010). Subduction controls of Hf and Nd isotopes in lavas of the Aleutian island arc. *Earth and Planetary Science Letters*, 300(3–4), 226–238. <https://doi.org/10.1016/j.epsl.2010.09.035>
- Zhang, Y. (1993). A modified effective binary diffusion model. *Journal of Geophysical Research: Solid Earth*, 98(B7), 11901–11920.
- Zhang, Y. (2010). Diffusion in minerals and melts: theoretical background. *Reviews in Mineralogy and Geochemistry*, 72(1), 5–59. <https://doi.org/10.2138/rmg.2010.72.2>
- Zhao, X., Zhang, Z., Huang, S., Liu, Y., Li, X., & Zhang, H. (2017). Coupled extremely light Ca and Fe isotopes in peridotites. *Geochimica et Cosmochimica Acta*, 208, 368–380. <https://doi.org/10.1016/j.gca.2017.03.024>